Articles

A Novel Defined PANoptosis-related Patterns For Predicting the Prognosis and Immune Characteristics in Kidney Clear Cell Carcinoma: Bioinformatics and Machine-learning Approach

Lixiong Zeng[1,#], Houyu Gan[1,#], Qiuli Chen[1,#], Delin Liu[1], Qian Guo[2], Fanyan Ou[3,*], Jie Yang[4,*], Kanglai Wei[1,*]

Abstract

Background: Renal clear cell carcinoma (KIRC) exhibits resistance to conventional therapies, and its heterogeneity limits the efficacy of immunotherapy. PANoptosis, as a key mechanism in personalized immunotherapy, has not yet been explored in KIRC. Our aim was to develop a prognostic model based on PANoptosis to predict immune responses and outcomes in KIRC patients. Methods: First, PANoptosis-related genes were identified, and RNA-sequencing data and clinicopathological features were collected from the TCGA-KIRC cohort. Subsequently, consensus clustering analysis was applied to identify distinct PANoptosis patterns. Prognosis-associated genes were then screened using univariate Cox regression. After feature selection via LASSO regression, a PANscore risk assessment system was constructed using multivariate Cox regression. The model was validated on the GSE29609 dataset to assess its predictive accuracy and generalizability. Furthermore, the relationship between PANscore and immune cell infiltration was analyzed, and pan-cancer analysis was performed. Finally, the predictive capabilities of traditional machine learning algorithms and convolutional neural network (CNN) algorithms were compared to determine the optimal prediction model. Results: Two distinct PANoptosis patterns were identified, with PANcluster 2 exhibiting superior potential for immunotherapy response. A novel prognostic indicator, named PANscore, was constructed to predict patients' clinical trajectories and treatment responses, with high-PANscore patients potentially benefiting more from immunotherapy. High PANscore was negatively correlated with most immune cell populations across multiple cancer types. In predicting patient outcomes based on PANoptosis-related gene expression, CNN outperformed traditional machine learning algorithms. Based on PANoptosis-related gene expression, KIRC was divided into two prognostically distinct PANoptosis patterns, PANcluster 1 and PANcluster 2, with PANcluster 1 showing a worse prognosis. The constructed PANscore risk model could predict prognosis and immune responses, with the high-PANscore group associated with advanced stages and immunosuppression. CNN significantly outperformed traditional algorithms in terms of AUC on the independent test set, suggesting that it may more effectively capture the nonlinear interactive features between PANoptosis-related genes and the immune microenvironment. Conclusion: Bioinformatics analyses suggest that PANcluster 2 and PANscore may serve as potential biomarkers for prognosis and immune responses in KIRC. In silico analyses further suggested a potential association between high PANscore and predicted benefit from immune checkpoint inhibitor therapy; however, this finding is hypothesis-generating and requires experimental and clinical validation. Machine learning approaches also showed exploratory potential as analytical and hypothesis-generating tools in this study. Collectively, our findings may provide a preliminary basis for future stratification of KIRC. Nevertheless, because all findings are based solely on bioinformatics analyses and have not been validated in experimental or clinical cohorts, PANscore should be considered a hypothesis-generating tool and a potential prognostic biomarker, and it is not yet ready to guide clinical decision-making. Prospective experimental and clinical validation is warranted.

Keywords: kidney clear cell carcinoma, PANoptosis, immune checkpoints, machine-learning approach

Article history: Submitted 10 March 2026 | Accepted 29 September 2026 | Published 27 October 2026

iCell, Vol. 3, No. 2 (2026): 128-147. DOI: https://dx.doi.org/10.71373/MLOH1115

Introduction

Renal cell carcinoma (RCC) ranks third among urogenital system cancers globally[1], with its incidence and mortality steadily increasing in recent years, expected to surpass 300,000 deaths by 2040[2]. In China, the estimated numbers of new cases and deaths from kidney cancer are 50,088 and 46,345, respectively[3]. According to a study based on age-period-cohort analysis, there is a significant increasing trend in kidney cancer mortality. Mortality rates have risen by 2.85% in males and 1.25% in females[4]. Renal cell carcinoma accounts for 90% of kidney cancer cases, with KIRC comprising 70%[5, 6]. KIRC is one of the most aggressive pathological types, with a worrisome prognosis, as approximately 45% of patients experience metastasis or recurrence after diagnosis[7], and among patients undergoing surgical treatment, 30% ultimately relapse[8].

[1]Department of Clinical Pathology, the Second Affiliated Hospital of Guangxi Medical University, Nanning, Guangxi, China. [2]Emergency Department, The First People's Hospital of Foshan, Foshan, Guangdong, China. [3]Department of Clinical Pathology, The First People's Hospital of Yulin, Yulin, Guangxi, China. [4]Clinical Medical Research Center, the Second Affiliated Hospital of Guangxi Medical University, Nanning, Guangxi, China.

#These authors contributed equally. *These authors are co-corresponding authors.

*Corresponding author: Kanglai Wei, Department of Clinical Pathology, the Second Affiliated Hospital of Guangxi Medical University, No. 166 University East Road, Xixiangtang District, Nanning, Guangxi, China. E-mail: yxwwkl@163.com

Genitourinary malignancies, such as prostate cancer[9] and bladder cancer[10], are typically managed with radiotherapy and chemotherapy. However, RCC remains the only genitourinary malignancy subtype demonstrating significant resistance to both radiotherapy and chemotherapy. Historically, RCC has been recognized as possessing intrinsic biological radioresistance, with early preclinical studies confirming that in vitro cultured RCC cells exhibit the most pronounced resistance to conventional radiation doses among all tumor cell types [11, 12]. Concurrently, RCC manifests inherently higher chemoresistance than most other malignancies[13], a multidrug-resistant phenotype arising from synergistic mechanisms: aberrant signaling pathway regulation[14], genetic aberrations[15,16], and cumulative oncogenic mutations[17] collectively constitute this complex resistance network, wherein the progressive accumulation of acquired mutations further reinforces the resistant phenotype. Notably, KIRC tumors display unique immune infiltration characteristics within their microenvironment, particularly abundant T-cell infiltration[18]. Through deepened understanding of tumor biology, the past decade has witnessed groundbreaking developments in vascular endothelial growth factor tyrosine kinase inhibitors, immune checkpoint blockers, and their combination therapies[19-21], establishing molecular targeted therapy and immunotherapy as indispensable strategies in clinical management[22]. Nonetheless, despite targeted therapy, immunotherapy, and the combined use of immune checkpoint inhibitors becoming the main treatment modalities for KIRC, personalized therapy is influenced by tumor heterogeneity and is effective only in a subset of patients[23,24]. The high heterogeneity of KIRC limits the implementation of persnonalized immunotherapy. Based on previous researches, We speculate that the differences in the effectiveness of immunotherapy among different patients may be related to immune escape, leading to some patients not benefiting from checkpoint blockade[25-27] .Therefore, there is an urgent need to identify reliable molecular biomarkers to predict the response to checkpoint blockade, enhance the clinical efficacy of these therapies, and predict patient prognosis.

PANoptosis serves as a pivotal programmed cell death mechanism within the innate immune system, encompassing pyroptosis, apoptosis, and necroptosis without being confined to a singular mode of cell death[28,29]. It elicits robust and sustained tumor-specific immune responses by dismantling cellular barriers and releasing danger-associated molecular patterns[30]. Current studies have revealed the dual role of PANoptosis in tumor immunity: In prostate adenocarcinoma, enhanced PANoptosis signaling has been demonstrated to potentiate overall anti-tumor immunity by promoting immune cell infiltration and upregulating immune checkpoint regulators[31]. However, in hepatocellular carcinoma, the low-risk group exhibits more favorable prognosis and distinct immune cell infiltration characteristics[32]. Similarly, gastric cancer research indicates that the low PANscore group demonstrates heightened sensitivity to immunotherapy[33]. These contradictory findings suggest that the impact of PANoptosis on immunotherapy exhibits cancer type-specific heterogeneity.

Building upon the aforementioned research background, it remains unclear whether PANoptosis promotes or suppresses immune responses in KIRC. In contrast to previous studies, our research systematically evaluates its role in KIRC for the first time by constructing a PANoptosis-related mRNA prognostic model. To validate the generalizability of this model, we further applied the risk stratification framework to pan-cancer analyses to predict differential responses to immunotherapy across various malignancies. This methodological approach not only extends prior understanding of PANoptosis heterogeneity but also employs machine learning to rigorously assess its predictive efficacy for KIRC prognosis.

Methods

Data acquisition and preprocessing

RNA-seq data and corresponding clinicopathological information for 542 KIRC samples were downloaded from the TCGA database (https://portal.gdc.cancer.gov/projects/TCGA-KIRC). Clinicopathological information and microarray expression profile data for the KIRC cohort GSE29609 were obtained from the GEO database (https://www.ncbi.nlm.nih.gov/geo/query/acc.cgi). To minimize systematic technical bias arising from cross-platform data integration, we extracted the overlapping gene set between the RNA-seq data from TCGA-KIRC and the microarray data from GSE29609. Subsequently, batch effects between the two platforms were jointly corrected using the ComBat function from the R package sva. This approach ensured that only shared genes were used for model validation, enhancing the reliability of cross-platform comparisons. Batch effects were corrected using the ComBat tool in R. Patients with survival times of less than 30 days were excluded to mitigate biases related to loss to follow-up or perioperative mortality. We confirm that the normalizeBetweenArrays function was applied separately and independently to the TCGA-KIRC training set and the GSE29609 test set, and was not applied globally to the combined TCGA + GEO data before splitting; therefore, no normalization or scaling parameters were estimated from the combined data, and the test set did not contribute to or borrow any parameters from the training set, so no data leakage occurred.

PANoptosis gene list

The PANoptosis-related mRNA gene list, comprising 66 genes with 26 from pyroptosis, 32 from apoptosis, and 8 from necroptosis, details its acquisition method and results in Table S1.

Survival analyses and construction of PANscore

Using the R package “survminer” for Kaplan–Meier survival analysis with log-rank test. Prognostic genes and independent predictors were identified through univariate and multivariate Cox proportional hazards regression analysis with the “survival” package. Prognostic hub genes underwent a least absolute shrinkage and selection operator (LASSO) regression model using the “glmnet” and “survival” packages. The coefficients for each gene were calculated with multivariate Cox analysis, and the selected genes were used to build the PANoptosis gene signature. PANscore was computed as the sum of gene expression products and corresponding coefficients. Patients were classified into high and low PANscore groups based on the optimal cut-off value determined by the “survminer” package.

Somatic mutation analysis

Downloaded from the TCGA database, somatic mutation data were analyzed with the "maftools" package in R. The tumor mutation burden (TMB) was calculated as the number of non-synonymous somatic mutations per megabase in cancer samples.

Immunotherapy response prediction and validation

Tumor immune dysfunction and exclusion (TIDE) is a computational framework developed to evaluate the potential of tumor immune escape from the gene expression profiles of cancer samples. The TIDE score, comprising immune dysfunction and immune exclusion components, can serve as a surrogate biomarker to predict the response to immune checkpoint blockade across various cancer types. More information about TIDE can be found at http://tide.dfci.harvard.edu/.

Immune cell infiltration analysis

Immune cell infiltration in 32 cancer types and in multiple KIRC datasets were calculated using seven algorithms, including TIMER[34], EPIC[35], xCELL[36], CIBERSORT[37], QUANTISEQ[38], MCPcount[39], and TIDE.

Machine-learning algorithms

LASSO is a regression technique that enhances model interpretability by penalizing absolute coefficient values, promoting sparsity. Random Forest (RF) is an ensemble method that builds multiple decision trees for robust predictions and feature importance insights. Support Vector Machine (SVM) with Recursive Feature Elimination (RFE) pairs the classification power of SVM with a feature selection process, iteratively refining models for optimal generalization.

Convolutional Neural Network

To convert one-dimensional gene expression data into a two-dimensional image matrix suitable for CNN input, this study identified 19 apoptosis-related differentially expressed genes based on the TCGA-KIRC and GSE29609 datasets. Gene expression data were normalized using the normalizeBetweenArrays function from the Limma package and transformed by log2(TPM+1). Meanwhile, the infiltration abundances of 10 immune cell types were estimated using the deconvo_mcpcounter function from the IOBR package, retaining the original proportional values. Given the complex co-expression and pathway regulatory relationships among genes, we performed an outer product operation between the 19 core gene expression profiles and the 10 immune cell infiltration abundances for each sample, constructing a 19×10 two-dimensional feature matrix to characterize the weighted activity of genes under specific immune contexts. This matrix was then converted into an RGB heatmap of 224×224 pixels using the pheatmap package in R, with gene expression values mapped to a color gradient. The entire process of normalization and heatmap generation was performed without using sample labels (high-risk vs. low-risk) to prevent data leakage. The CNN model was built using the Keras Sequential API, with an input layer of size $(19, 10, 1)$. The convolutional layer was configured with 16 filters of 3×3 kernels (stride 1, same padding, ReLU activation). After flattening, a fully connected layer with 16 neurons (ReLU activation, dropout rate 0.3) was added, followed by an output layer with 1 neuron and sigmoid activation to output the five-year mortality probability. Hyperparameters were optimized via random search, and the optimal combination was determined based on maximizing the AUC on the validation set, which included 16 3×3 convolutional filters, 16 fully connected neurons, a learning rate of 1e-5, a dropout rate of 0.3, and a batch size of 16. Training used binary cross-entropy loss and the Adam optimizer (learning rate 0.00001) with a batch size of 16, for a maximum of 1000 epochs, with 20% of the data held out for validation. Early stopping was applied (training terminated if validation loss showed no improvement for 15 consecutive epochs, restoring the best weights). Meanwhile, AUC, F1-score, and recall were monitored. L2 regularization ($\lambda = 0.001$) and dropout were applied before and after the fully connected layer to prevent overfitting. The final model was independently tested on the heatmaps of 39 GSE29609 samples, and an ROC curve was plotted to evaluate its performance.

We used the `normalizeBetweenArrays` function in the Limma package to separately normalize the TCGA-KIRC and GSE29609 datasets. Then, we used the `deconvo_mcpcounter` function in the IOBR package to perform MCP-counter algorithm calculations on the TCGA-KIRC and GSE29609 datasets, estimating the infiltration abundance values of ten immune cell types for each sample. PANoptosis-related differentially expressed genes were screened based on the TCGA training cohort. To ensure cross-platform applicability, we confirmed that these genes were detectable on the GSE29609 microarray platform, and ultimately 19 genes met the above conditions. Subsequently, we performed element-wise multiplication between the infiltration abundance values of the ten immune cell types and the expression levels of the 19 genes for each sample, and generated heatmaps based on the results. Finally, we obtained 533 TCGA-KIRC and 39 GSE29609 heatmaps as model input files, with the corresponding outcome of whether death was due to tumor as the result file.

Then, we used the Sequential model in the Keras library to construct a CNN-based binary outcome prediction model. Input layer: a two-dimensional convolutional layer (Conv2D) containing 16 3×3 kernels, with ReLU activation, and an input data shape of (19, 10, 1). This layer used `padding='same'` to keep the input and output dimensions consistent. Flatten layer: a Flatten layer was used to flatten the output of the two-dimensional convolutional layer into a one-dimensional vector, facilitating connection to the fully connected layers. Fully connected layers: the first fully connected layer contained 16 neurons with ReLU activation. The final fully connected layer contained 1 neuron with sigmoid activation, used to output the binary classification result. We used the Adam optimizer with a learning rate of 0.00001. The loss function was binary crossentropy, and the metric was accuracy. The 533 TCGA-KIRC heatmaps were used as the training set. The model was trained on the training set for 1000 iterations, with 20% of the data used for validation, and the accuracy, error rate, F1 score, and recall were recorded at each iteration. Finally, the 39 GSE29609 heatmaps were used as the test set to evaluate the final model, and ROC curves were plotted. They overlap with the 7 LASSO-screened genes or the 3 final PANscore genes; the three machine learning methods we used were developed from genes screened from the TCGA differentially expressed genes.

Statistical analysis

Statistical analysis was performed using R software (version 4.1.0) and the Sangerbox tool (http://www.sangerbox.com/tool). Continuous variables are presented as mean ± standard error of the mean (SEM). The normality of data distribution was assessed using the Shapiro–Wilk test, and homogeneity of variances was evaluated using Levene's test. For data that were normally distributed with equal variances, comparisons between two groups were performed using Student's t-test, and comparisons among multiple groups were performed using one-way analysis of variance (ANOVA). For non-normally distributed data, comparisons between two groups were performed using the Wilcoxon rank-sum test, and comparisons among multiple groups were performed using the Kruskal–Wallis test. For all multiple-group comparisons, the Benjamini–Hochberg false discovery rate (FDR) method was uniformly applied for multiple comparison correction, with significance set at FDR < 0.05. Categorical data were compared using the chi-square test or Fisher's exact test. All statistical tests were two-sided, and the significance level was set at $P < 0.05$, with $*P < 0.05$, $**P < 0.01$, and $***P < 0.001$ denoting the corresponding levels. Continuous variables are presented as mean ± standard error, and comparisons were performed using Student's t-test or the Wilcoxon rank-sum test. Categorical data were compared using the chi-square test. Statistical significance was set at $P < 0.05$, with $*P < 0.05$, $**P < 0.01$, and $***P < 0.001$ indicating the respective significance levels.

Results

Expression, prognostic significance and interaction of PANoptosis genes and Characterization of PANoptosis patterns

This investigation is encapsulated in a visual synopsis (Fig 1). The PANoptosis gene list comprises 66 genes, including 26 genes from pyroptosis, 32 genes from apoptosis, and 8 genes from necroptosis (Table 1). For the genes in question, an interaction network among proteins was mapped out via the String online tool (Fig. 2A). To facilitate molecular categorization related to PANoptosis, a meta-analysis cohort of KIRC was formed, pooling data from 542 KIRC subjects across TCGA-KIRC groups. Conducting a univariate Cox regression within this meta-cohort highlighted 40 genes whose expression significantly tied to KIRC patient survival. Specifically, 20 genes indicated a positive prognosis, mirroring another 20 that suggested a negative outlook (Fig. 2B). Through consensus clustering driven by PANoptosis gene expression data, the meta-cohort bifurcated into two unique PANoptosis profiles, dubbed PANclusters 1 and 2, with counts of 383 and 159 patients, respectively (Fig. 2C). Principal component analysis (PCA) underscored divergent transcriptomic attributes between these clusters (Fig. 2D). Kaplan-Meier analysis pointed to PANcluster 1 as having the least favorable survival statistics ($P = 0.021$) (Fig. 2E). Further analysis revealed that the majority of PANoptosis-related genes were significantly upregulated in both cohorts (Figure 2F).

Molecular characteristics and biological functions in different PANoptosis patterns

We analyzed somatic mutations in distinct PANoptosis patterns within the TCGA-KIRC cohort. PANcluster 1 had a lower mutation rate of 82.64% compared to 89.42% in PANcluster 2 (Fig. 3A, B). Both clusters showed increased mutation rates for VHL, *PBRM1*, and TTN. No significant differences in TMB and MSI were observed between the two clusters (Fig. 3C-D). GO enrichment analysis revealed significant enrichment of immune-related pathways in the Biological Process domain for both clusters, including regulation of leukocyte-mediated immunity and cytokine production. In the Cellular Component domain, enrichment was primarily in the plasma membrane exterior and collagenous extracellular matrix. For Molecular Function, both clusters were enriched in metal ion transmembrane transport and monatomic ion channel activity (Fig. 3E-F). Immune checkpoint gene expression analysis showed elevated expression in most genes in PANcluster 2, except for BTNL9 and TNFRSF14 (Fig. 3G).

Construction and validation of PANoptosis scoring system (PANscore)

To address the limitations of individual risk assessment based on retrospective genomic analysis of PANoptosis patterns, we developed a PANscore risk scoring system specifically for KIRC patients. In the TCGA-KIRC training cohort, univariate Cox regression analysis identified 7 PANoptosis-related genes associated with prognosis (Figure 4A); interestingly, all of them were derived from the 40 genes screened in Section 2.1. LASSO regression was further applied for dimensionality reduction (Figure 4B-C). Kaplan-Meier analysis demonstrated that high expression of *CASP4* , *DIABLO*, *PYCARD*, *E2F1*, *TRAF2*, and *LY96* was associated with poor prognosis, whereas high expression of *UNC5B* indicated a better prognosis (Figure 4D-J). Ultimately, a three-gene signature was constructed using multivariate Cox regression analysis: PANscore = $CASP4 \times 0.0206 + E2F1 \times 0.0257 + UNC5B \times (-0.006)$. After stratification by the optimal cut-off value, patients with a high PANscore in the training cohort exhibited significantly worse prognosis ($P = 0.004$, Figure 4K), and this finding was consistently validated in the independent validation cohort (GSE29609; $P < 0.001$, Figure 4L).

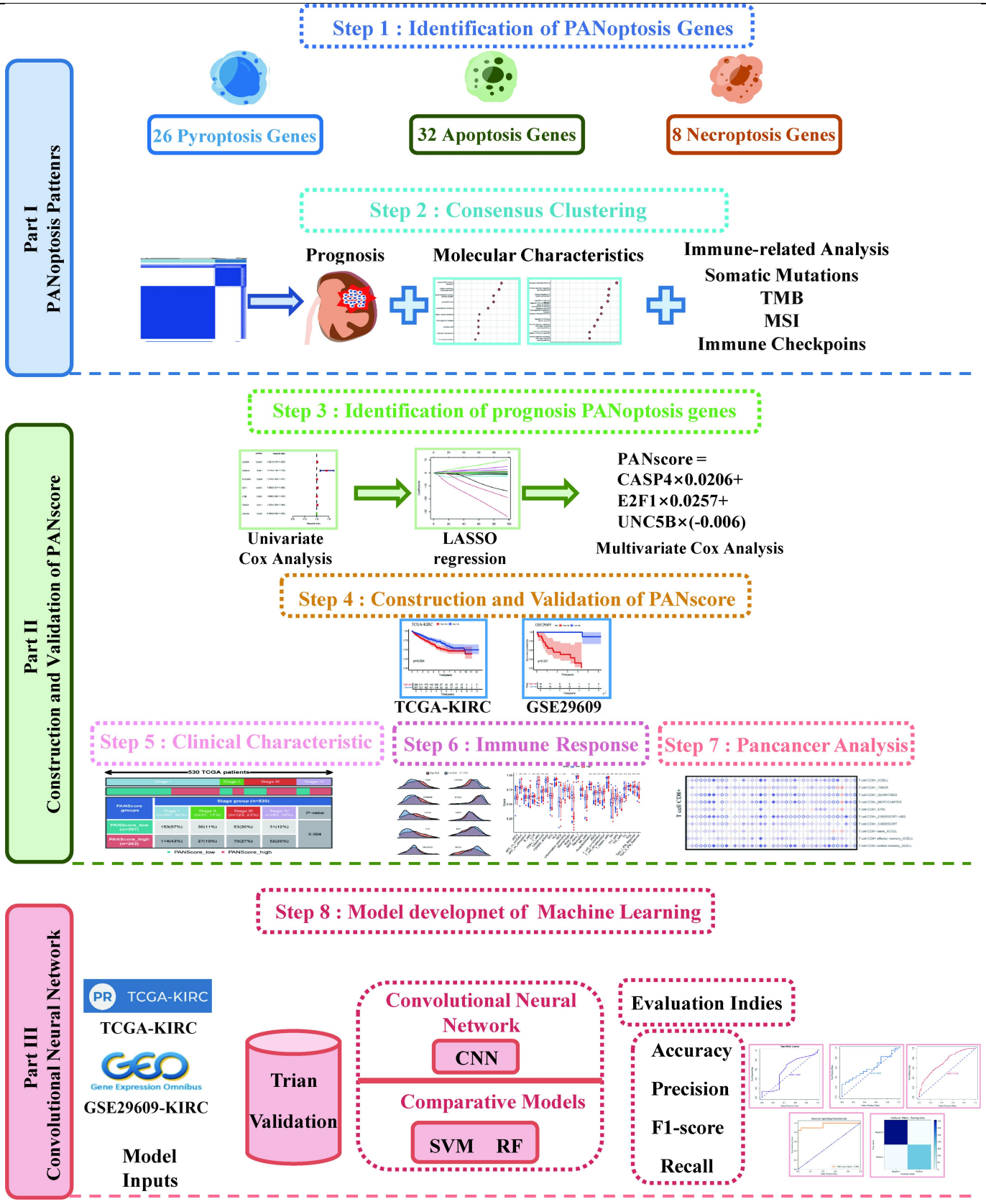


Figure 1. Figure 1 A graphic abstract of this study.

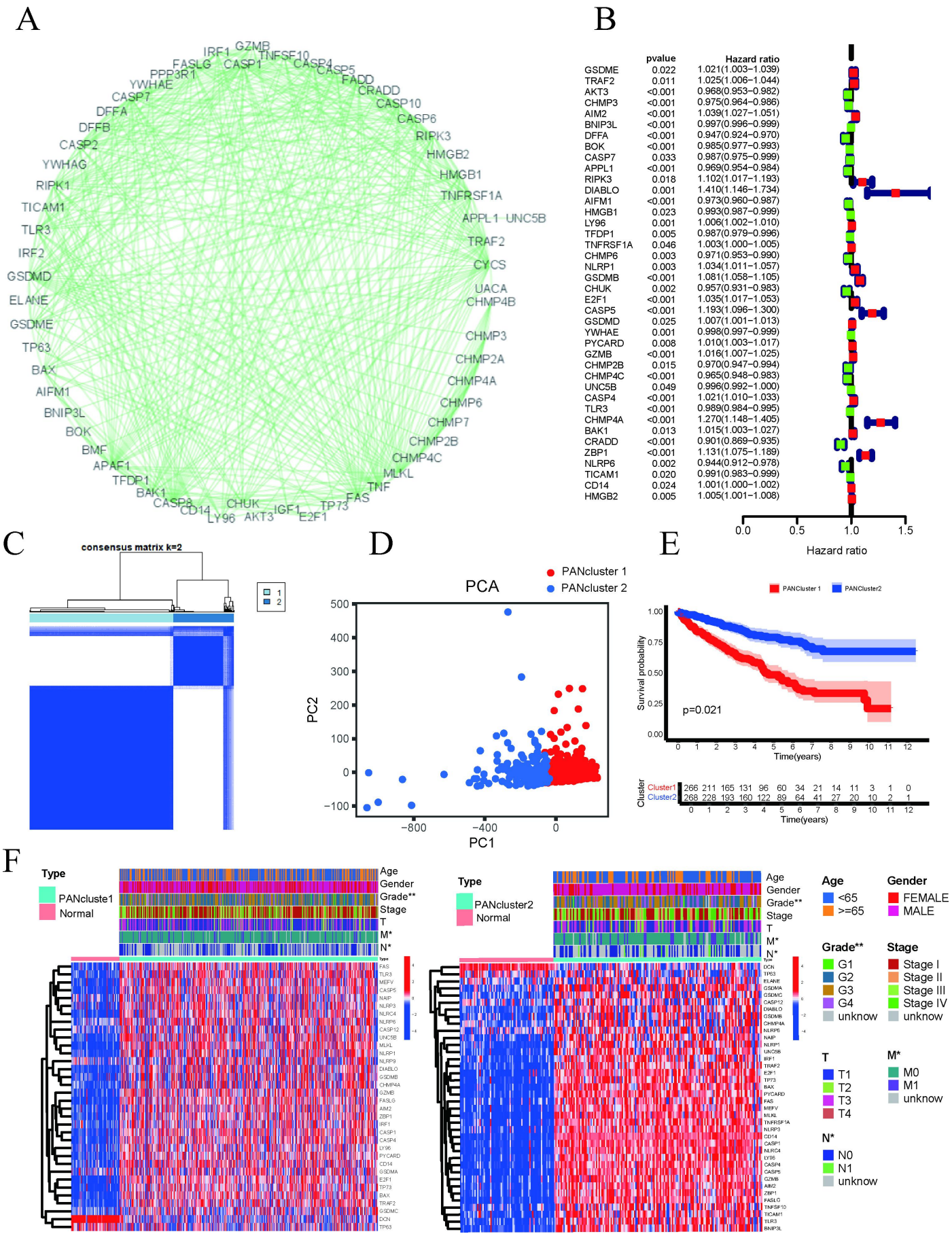


Figure 2. Expression, prognostic significance, and interaction of PANoptosis genes and Characterization of PANoptosis patterns. (A) PPI network of 66 PANoptosis-associated genes; (B) Univariate analysis; (C) Consensus clustering; (D) PCA (Principal Component Analysis); (E) Kaplan-Meier survival analysis; (F) Heatmap of PANoptosis genes and their clinical pathological characteristics.

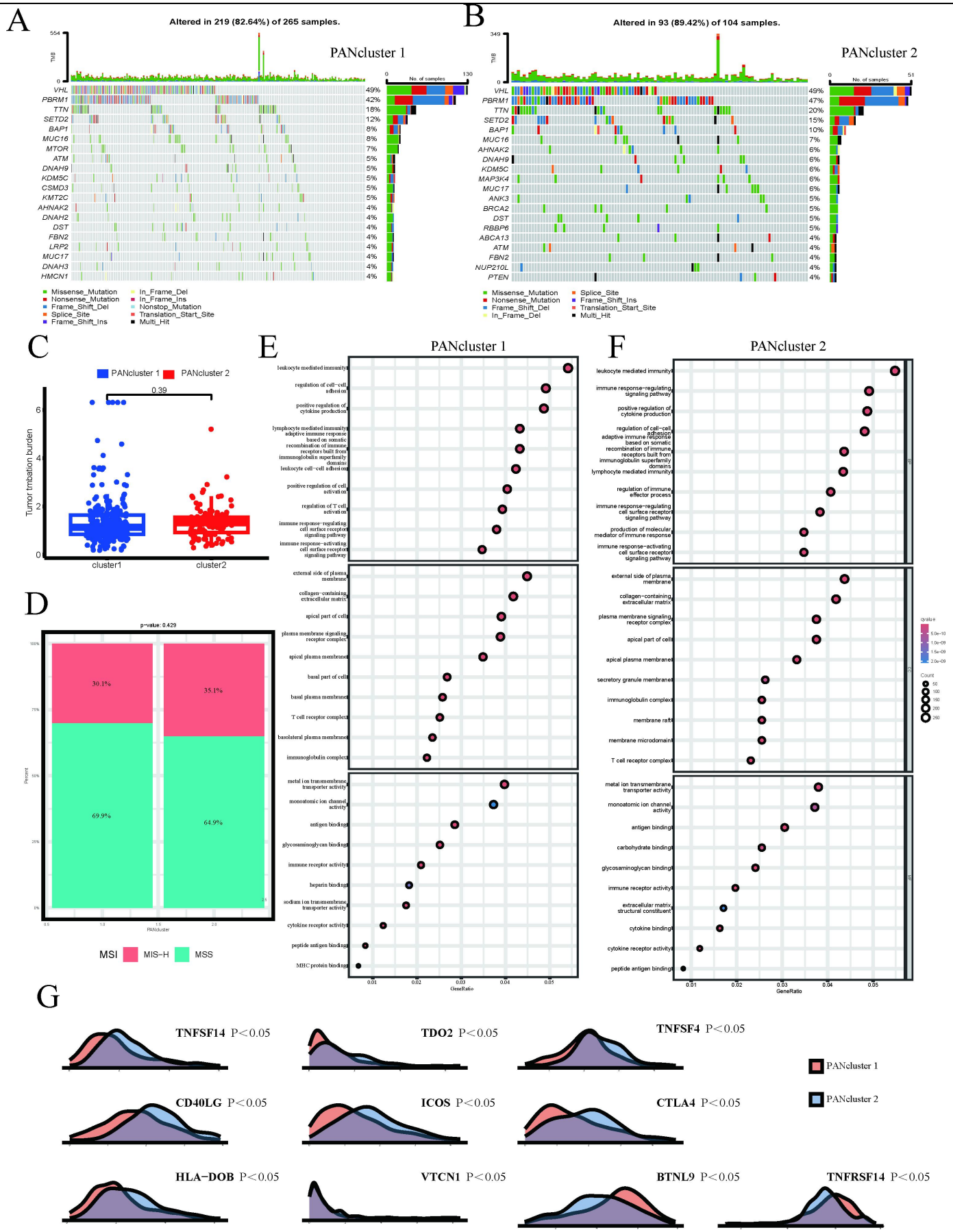


Figure 3. Molecular characteristics and biological functions in different PANoptosis patterns. (A) Somatic mutations in PANcluster 1; (B) Somatic mutations in PANcluster 2; (C) TMB (Tumor Mutational Burden); (D) MSI (Microsatellite Instability); (E) Gene Ontology (GO) analysis for PANcluster 1; (F) GOanalysis for PANcluster 2; (G) Immune checkpoints in different PANclusters.

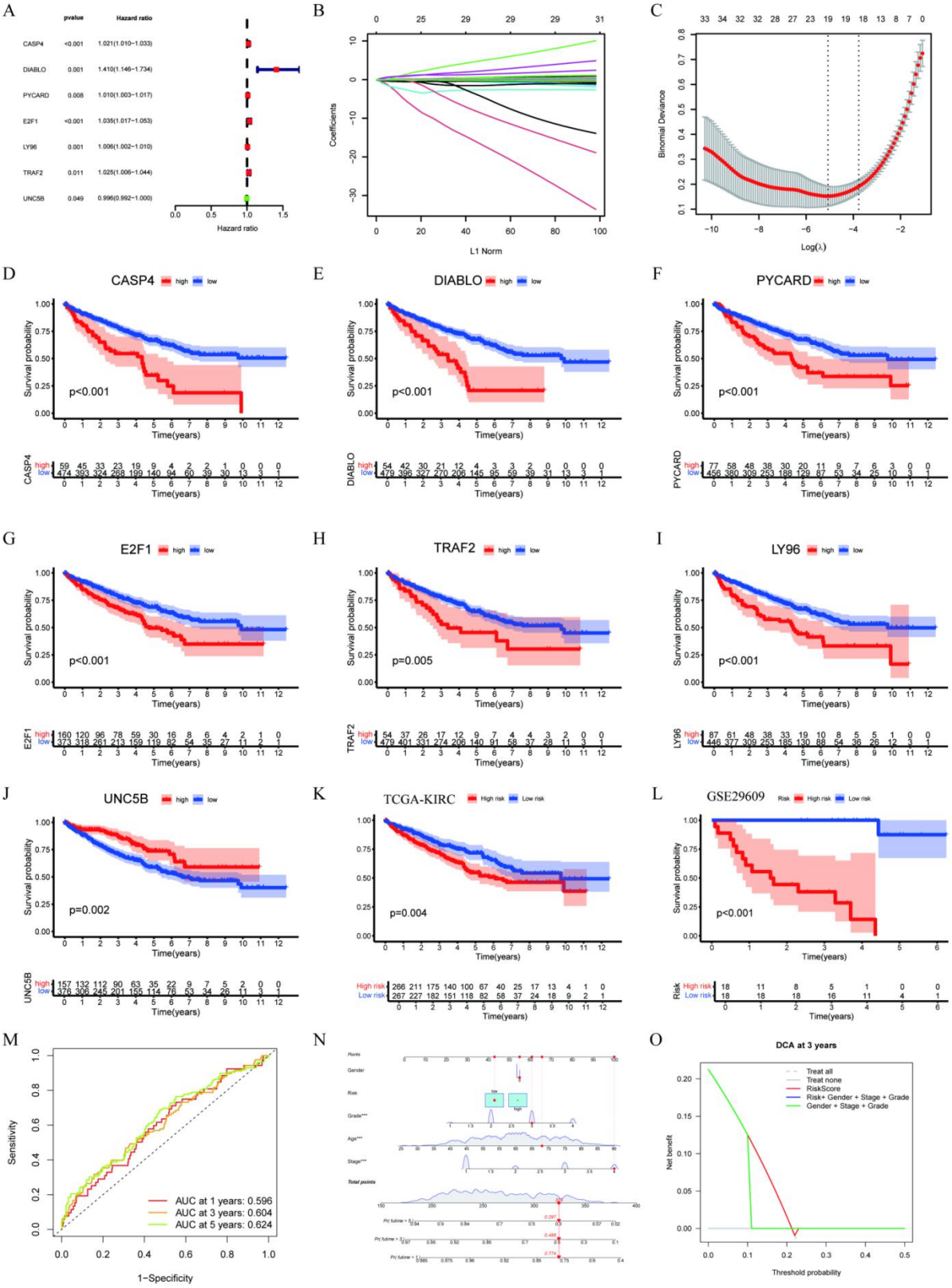


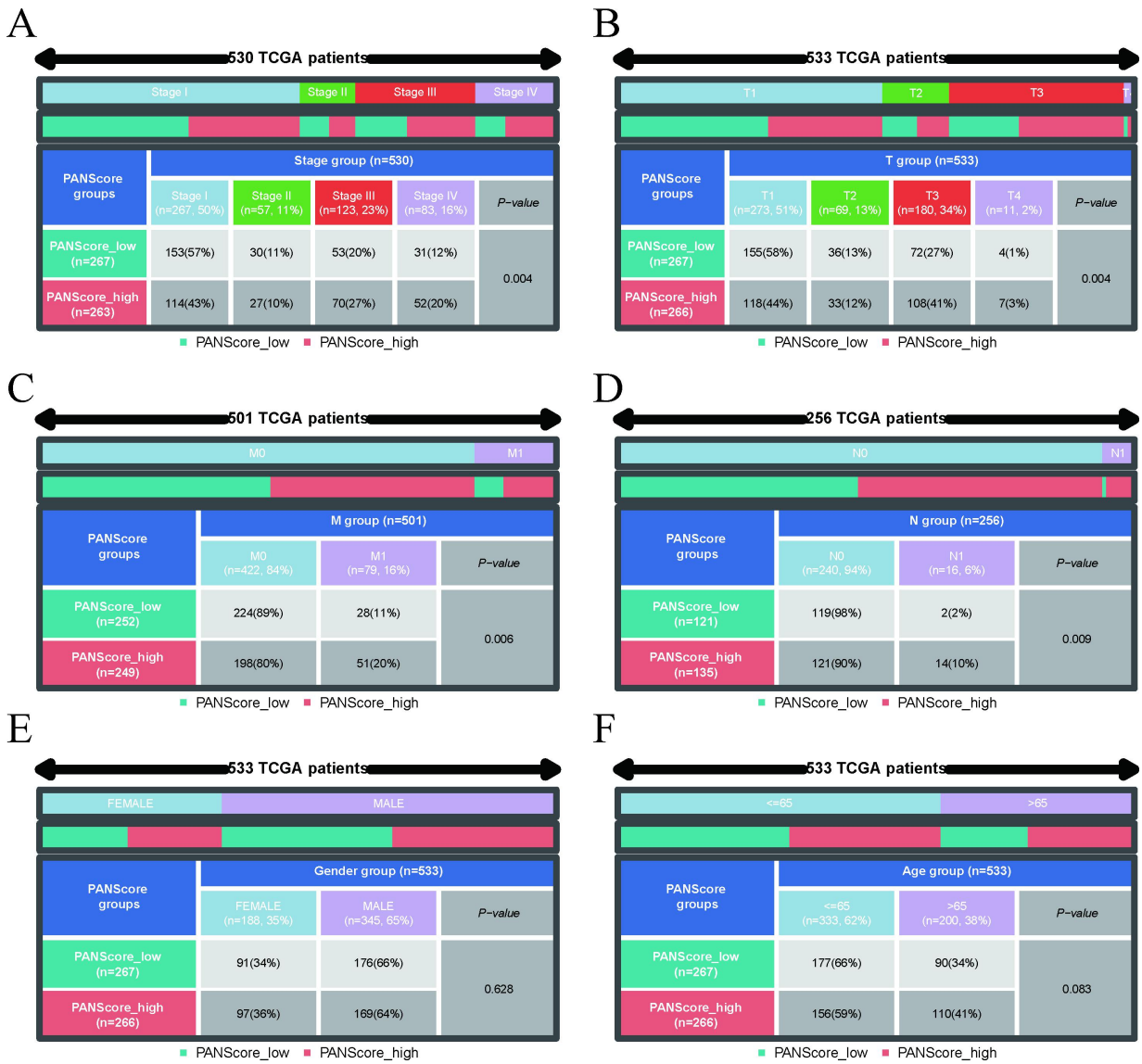
Figure 4. Construction and validation of the PANoptosis scoring system (PANscore). (A) Univariate Cox analysis of 7 prognostic PANoptosis genes in TCGA-KIRC. (B-C) Dimensionality reduction using LASSO regression analysis with survival data from the TCGA-KIRC training set. Kaplan-Meier survival analysis indicating that *CASP4* (D), *DIABLO* (E), *PYCARD* (F), *E2F1* (G), *TRAF2* (H), and *LY96* (I) were significantly associated with a worse prognosis, whereas high expression of *UNC5B* (J) was associated with a better prognosis. Kaplan-Meier analysis demonstrated that patients with a high PANscore had a significantly worse prognosis (K). The validation set (GSE29609) also showed that a high PANscore was associated with a worse prognosis (L). (M) Time‐dependent ROC; (N) Nomogram integrating PANscore with clinical factors for survival prediction, with good calibration. (O) DCA showed PANscore added net benefit over the clinical model alone.

To further refine the construction and address the limitations of individual risk assessment, we developed a KIRC-specific PANscore risk scoring system. First, prognosis-related PANoptosis genes were screened by univariate Cox regression and LASSO regression,

and the intersection yielded a candidate set of 7 genes: *CASP4*, *DIABLO*, *PYCARD*, *E2F1*, *LY96*, *TRAF2*, and *UNC5B*, all of which originated from the 40 core PANoptosis genes previously identified (Figure 4A-C). Kaplan-Meier analysis confirmed that high expression of *CASP4*, *DIABLO*, *PYCARD*, *E2F1*, *TRAF2*, and *LY96* was significantly associated with poor prognosis, while high UNC5B expression indicated a more favorable prognosis (Figure 4D-J). Subsequently, these 7 genes were incorporated into a multivariate Cox proportional hazards model, and variable selection was performed using bidirectional stepwise regression based on the Akaike Information Criterion (AIC). The most parsimonious optimal subset consisting of *CASP4*, *E2F1*, and *UNC5B* was ultimately determined, which yielded the minimum AIC value. Accordingly, the three-gene risk score formula was constructed as: PANscore = *CASP4* × 0.0206 + *E2F1* × 0.0257 + *UNC5B* × (−0.006). Following risk stratification by the optimal cut-off, patients with a high PANscore in the training cohort (TCGA- KIRC) demonstrated significantly worse prognosis ($P = 0.004$, Figure 4K), and this result was consistently validated in the independent validation cohort (GSE29609; $P < 0.001$, Figure 4L). To further evaluate the predictive performance and clinical utility of the PANscore, we additionally performed time- dependent ROC analysis, nomogram calibration, and decision curve analysis (DCA). The time-dependent ROC curves revealed that the discriminatory ability of the PANscore gradually improved with extended follow-up time: the 1-year AUC was 0.596, the 3-year AUC was 0.604, and the 5-year AUC was 0.624 (Figure 4M), suggesting that PANoptosis- related gene expression patterns have superior predictive value for long-term survival outcomes in KIRC patients compared to short-term prognosis. We further constructed a nomogram integrating the PANscore with Gender, Grade, Age, and Stage (Figure 4N). This model enabled individualized risk quantification by summing the points assigned to each variable to obtain total points, corresponding to 1-, 3-, and 5-year survival probabilities. Calibration curves showed that as total points increased, the predicted survival probabilities exhibited a monotonic decreasing trend, which was highly consistent with the clinical course of KIRC, indicating good calibration of the integrated model. Decision curve analysis (DCA) demonstrated that the PANscore alone provided a net benefit within the threshold probability range of 0.05–0.22; in contrast, the clinical model without the PANscore (Gender + Stage + Grade) lost net benefit at a threshold probability of approximately 0.1 (Figure 4O), further confirming the added value of the PANscore from a clinical utility perspective.

Clinicopathologic characteristics of the PANscore groups

Additionally, we examined the clinicopathological features associated with PANscore stratification in the meta-KIRC cohort. Our analysis revealed a significant correlation between high PANscore and advanced TNM staging (Fig. 5A-D). However, no significant differences were observed in gender or age distribution between the low and high PANscore groups (Fig. 5E-F).



iCell Vol. 3 No. 2 (2026): 128-147

Figure 5. Clinicopathologic characteristics of the PANscore groups. Characteristics of STAGE classification (A), T classification (B), M classification (C), N classification (D), gender (E), and age (F) among different PANscore groups.

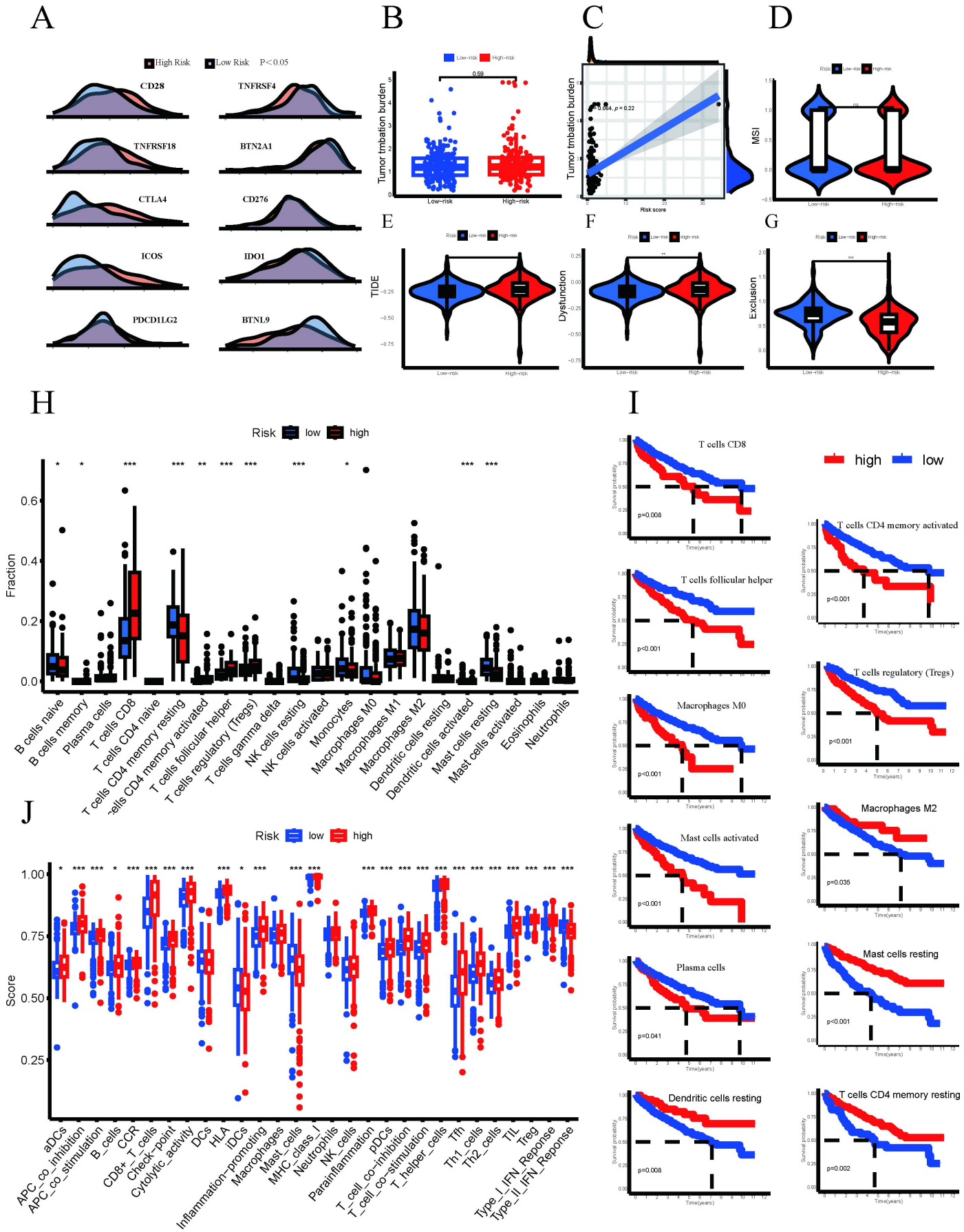


Figure 6. Molecular and immune characteristics of different PANscore groups. Immune checkpoint (A), TMB (B-C), MSI(D), tumor immunity dysfunction and exclusion (E-G), immune cell analysis (H-I), and immune function analysis using ssGSEA (J) between different PANscore groups.

Immunological correlation of PANscore in pancarcinoma

We assessed immune cell infiltration across 32 cancer types (including subtypes) employing seven distinct algorithms (Fig. 7 and Table S2). Our analysis revealed a significant negative correlation between PANscore and various immune cells, including T cell CD8+, T cell CD4+, Tδ cells, Tregs, Tfh, B cells, NK cells, macrophages, macrophage M1, monocytes, neutrophils, and dendritic cells. Conversely, a significant positive correlation was observed between PANscore and macrophages M0 and M2. These findings indicate that PANoptosis significantly influences the tumor immune microenvironment in a broad spectrum of cancers.

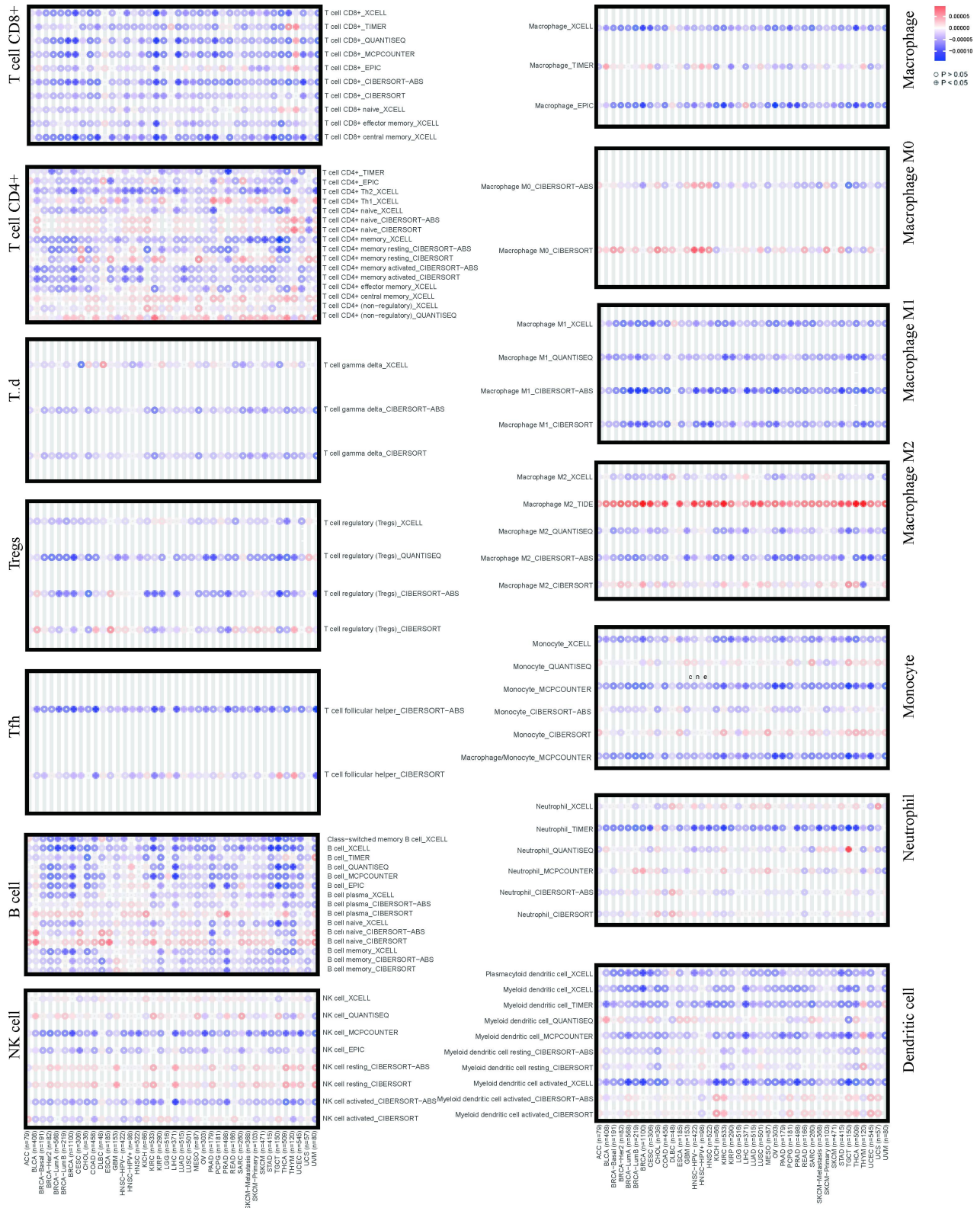


Figure 7. Immunological correlation of PANscore in pancarcinoma.

Assessment of prognostic accuracy of PANoptosis gene pairs in KIRC using machine-learning algorithms and Convolutional Neural Networks

In the present study, we initially employed three traditional machine learning algorithms—LASSO regression, random forest, and SVM-RFE —to analyze PANoptosis-related genes and construct prognostic prediction models for KIRC. The results indicated that LASSO regression (11 genes, AUC = 0.630), random forest (19 genes, AUC = 0.587), and SVM-RFE (5 genes, AUC = 0.601) (Fig. 8A-I) could predict the prognosis of KIRC patients to a certain extent. However, these algorithms may struggle to fully uncover the complex interrelationships among genes when processing complex genomic data, thereby limiting further improvement in their predictive performance. Given the limitations of traditional machine learning algorithms, we subsequently introduced a deep learning algorithm, CNN, which has the capability to automatically extract complex data features and better capture the nonlinear relationships and higher-order interactions among genes. The results demonstrated that CNN achieved higher accuracy on the test set (AUC = 0.96, Fig. 8J-O), significantly outperforming traditional machine learning algorithms. This finding suggests that, in the prognostic prediction of KIRC based on PANoptosis-related genes, CNN has a distinct advantage and can more accurately assess the prognostic risk of patients.

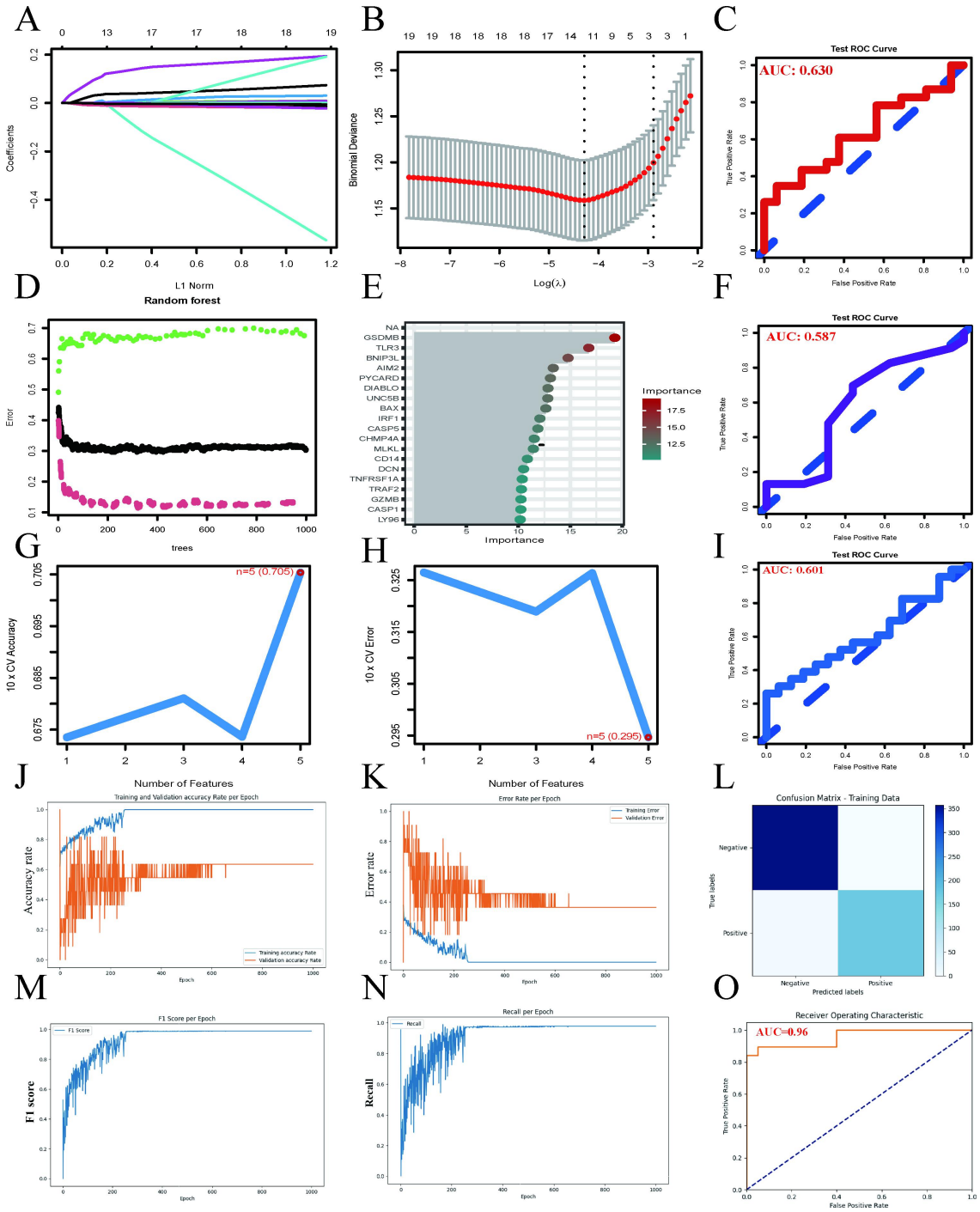


Figure 8. Assessment of prognostic accuracy of PANoptosis gene pairs in KIRC using machine-learning algorithms and CNN. LASSO identified 11 prognostic genes (A-B) with an AUC-ROC curve in (C). RF selected 19 genes (D-E) and its AUC-ROC curve is in (F). SVM+RFE identified 5 genes (G-H) with AUC-ROC curve in (I). CNN analysis demonstrated accuracy, error rate, F1 score, recall rate, and AUC-ROC in (J-O).

Discussion

This study marks a pioneering application of traditional machine learning techniques—LASSO, RF, and SVM combined with RFE—alongside CNN, in assessing the precision of PANoptosis-related gene sets for predicting outcomes in KIRC patients. The main findings are summarized as follows: First, two distinct PANoptosis patterns were identified, among which PANcluster 2 may suggest a higher responsiveness to immunotherapeutic intervention. PANcluster 1 exhibited the worst survival statistics, and most immune checkpoint genes showed elevated expression in PANcluster 2. Subsequently, a robust PANscore metric was constructed that effectively predicted prognosis and immunotherapy response in KIRC patients, suggesting that patients with a high PANscore may derive greater benefit from immune checkpoint inhibitor therapy than those with a low PANscore. Patients in the high-PANscore group had significantly worse prognosis, displayed higher TIDE scores and immune dysfunction, with $CD8^+$ T cells potentially in an exhausted state, while immune exclusion was negatively correlated with a high PANscore, indicating a possible attenuated or suppressed immune status. If immune checkpoint inhibitor monotherapy is likely to induce resistance, combination therapy may effectively reverse this and activate $CD8^+$ T cells, thereby conferring more pronounced clinical survival benefits compared to the low-risk population. Furthermore, pan-cancer analysis revealed significant negative correlations between the high-PANscore cohort and most immune cell populations. Finally, compared with traditional machine learning approaches, CNN demonstrated markedly higher accuracy in predicting KIRC patient outcomes based on PANoptosis-related gene sets. However, it must be emphasized that all findings in this study were derived from public transcriptomic datasets and have not yet been validated using human clinical specimens, primary renal tubular cells, or in vivo animal tumor models. Therefore, the clinical applicability of the PANscore for guiding immunotherapeutic decisions remains preliminary, and rigorous validation in independent multi-cohort studies and prospective clinical trials is required before any translational application.

The multi-algorithm collaborative strategy adopted in this study was motivated by the complementary strengths of the selected methods. LASSO regression enables efficient feature selection in high-dimensional genomic data through L1 regularization; random forest is well suited to capturing complex nonlinear relationships among genes; SVM-RFE is particularly useful for feature optimization in small-sample, high-dimensional datasets; and CNN can automatically identify latent spatial patterns in genomic data. For model evaluation, AUC was used as the primary metric, supplemented by error rate and accuracy. Rigorous cross-validation and internal validation were performed to assess the reliability of the results within the available dataset. This integrative strategy helps mitigate the limitations of individual models and may allow more comprehensive exploration of the predictive potential of the PANoptosis gene set. However, because the input feature spaces differed among the models—particularly between the traditional machine learning models and the CNN—the comparison should be interpreted with caution, and the apparent advantage of CNN may be partly attributable to its access to multimodal features rather than to its architecture per se. In this study, the CNN model achieved a relatively high AUC (0.96) in a small sample (n = 39); as the reviewer correctly noted, this validation was performed on the training set rather than an independent test set. This result should therefore be interpreted cautiously, as it may stem from small-sample bias and artificial data transformation. Although cross-validation and early stopping were adopted, the risk of overfitting cannot be completely ruled out, and this performance requires further validation in larger independent cohorts.

Emerging research indicates that PANoptosis has diverse effects on immunotherapy responses in various cancers. However, the exact influence of PANoptosis on immunotherapy outcomes in KIRC remains unclear. Although investigations have touched upon PANoptosis-associated long non-coding RNAs (lncRNAs)[40] and microRNAs (miRNAs)[41] in KIRC that correlate positively with immune functions, it is crucial to recognize that lncRNAs and miRNAs exert their regulatory effects on gene expression and function by influencing mRNA levels. As pivotal molecules in cellular communication, mRNAs directly impact the function of immune cells and the modulation of immune responses. Yet, the specific roles of mRNAs associated with PANoptosis in the immune response of KIRC are not well elucidated. Consequently, we have devised an mRNA-based algorithmic model linked to PANoptosis to forecast the prognosis of KIRC patients, offering insights into immunotherapy and serving as a guide for the development of future personalized treatment approaches.

We initially pinpointed genes linked to PANoptosis and discerned two unique PANoptosis patterns. Patients within PANcluster 1 faced the most unfavorable prognosis. Regarding immune checkpoints, those in PANcluster 2 showed elevated expression in specific checkpoints, suggesting a potentially superior response to immunotherapy. Thus, classifying patients by PANoptosis patterns could facilitate personalized treatment planning. Both patterns exhibited significant enrichment in immune-related pathways. Furthermore, mutation analysis of PANoptosis genes aids in pinpointing therapeutic targets and resistance mechanisms. Notably, VHL, *PBRM1*, and TTN showed high mutation rates across both patterns. Research indicates that VHL mutations in KIRC impede immune molecule efflux and adhesion[42]. Additionally, KIRC with *PBRM1* mutations may exhibit enhanced responsiveness to PD-1 inhibitors[43]. While the upregulation of lncRNA TTN-AS1, transcribed antisense from the TTN gene, correlates with adverse clinical traits in KIRC, the connection between TTN mutations and immune responsiveness warrants further exploration[44].

In this study, we developed and validated a personalized risk assessment tool for KIRC, designated as PANscore. First, univariate Cox analysis identified seven prognostic PANoptosis-related genes. Subsequently, LASSO regression analysis was employed to construct a three-gene signature. Specifically, prognosis-related genes were separately screened by univariate Cox regression and LASSO regression, and the intersecting genes were then incorporated into a multivariate Cox proportional hazards model, followed by bidirectional stepwise regression based on the AIC for variable selection to obtain the most parsimonious predictive model. Ultimately, an optimal subset consisting of three genes—*CASP4*, *E2F1*, and *UNC5B*—was determined, which yielded the minimum AIC value. The established scoring formula was: PANscore = $CASP4 \times 0.0206 + E2F1 \times 0.0257 + UNC5B \times (-0.006)$. This calculated PANscore enables rapid and accurate identification of patient risk levels, stratifying patients into low-risk and high-risk groups. Kaplan–Meier analysis demonstrated that patients with a high PANscore had significantly worse

prognosis. The three genes constituting the PANscore signature, *CASP4*, *E2F1*, and *UNC5B*, may function through interconnected pathways mediating PANoptosis and immune evasion in KIRC. *CASP4* is a key mediator of pyroptosis, whose activation triggers an inflammatory caspase cascade that induces immunogenic cell death. *E2F1* is a transcription factor involved in cell cycle regulation and apoptosis, and has been shown to regulate *CASP4* expression, suggesting a direct regulatory link between apoptotic and pyroptotic pathways. *UNC5B* is a netrin-1 receptor that acts as a dependence receptor, inducing apoptosis in the absence of its ligand. In KIRC, UNC5B expression is downregulated, and its loss may promote tumor progression by releasing cells from dependence receptor-mediated apoptosis. The synergistic interactions among these genes may form a PANoptosis signaling network: *E2F1*-mediated transcriptional activation of *CASP4* promotes pyroptosis, while *UNC5B*-mediated apoptosis provides an additional cell death pathway. When both pathways are dysregulated, tumor cells may evade PANoptosis while simultaneously creating an immunosuppressive microenvironment through chronic inflammation and checkpoint upregulation. Thus, this three-gene signature captures the complex interplay between distinct programmed cell death pathways and immune evasion in KIRC. Recent studies have linked high expression of *CASP4* and *E2F1* to increased immune cell infiltration in KIRC and have also shown that these genes promote the malignant progression of KIRC [45, 46], indicating their multifaceted roles in KIRC development. Additionally, *UNC5B* is suggested to inhibit KIRC development[47], though its impact on the immune response in KIRC remains unexplored. Kushal et al. found that the interaction between *FLRT3* and *UNC5B* suppresses T cell activity, facilitating tumor escape, and that blocking this pathway could enhance immunotherapy efficacy. Immunohistochemistry confirmed that *FLRT3* is highly expressed in KIRC, suggesting that targeting the *FLRT3*-*UNC5B* pathway might benefit KIRC patients unresponsive to current treatments[48]. However, it should be noted with caution that the current PANscore model was constructed using LASSO-Cox regression based on the single-cancer training cohort TCGA-KIRC, and its gene weight coefficients reflect the specific molecular context of KIRC rather than an optimal solution at the pan-cancer level. The prognostic directions of these genes may exhibit biological heterogeneity across different cancer types, potentially varying across distinct tumor backgrounds due to tissue-specific expression patterns, differences in the tumor microenvironment, and cancer-type-specific immune evasion mechanisms. Therefore, direct application of the KIRC-derived PANscore formula in pan-cancer analyses may suffer from inherent cancer-type specificity limitations regarding its extrapolation validity. The application of the PANscore model to cancer types other than KIRC should be interpreted with caution, and future studies should validate and potentially recalibrate the model for specific cancer types.

In this study, although PANclusters and PANscore were derived from different analytical approaches, both were based on PANoptosis-related gene expression data and are inherently interconnected. PANclusters were identified via consensus clustering as two distinct PANoptosis patterns with significantly different prognoses (PANcluster 1 was associated with worse prognosis), whereas PANscore was constructed as a quantitative risk assessment system comprising three key genes through LASSO-Cox regression analysis. These two methods are complementary: PANclusters reveal population heterogeneity, while PANscore provides individualized risk assessment. In clinical application, the combination of PANclusters and PANscore not only captures overall characteristics but also enables precise prognostic prediction, offering a dual basis for personalized treatment strategies in KIRC patients. PANcluster stratifies patients by gene expression, providing a qualitative classification of PANoptosis patterns and revealing population heterogeneity, whereas PANscore stratifies patients by model-derived scores, offering a quantitative and individualized risk assessment. These two systems are complementary rather than contradictory; however, the intrinsic correlation between the two classification systems is not yet fully elucidated, and the PANcluster groups may contain samples with both high and low PANscore values. PANcluster 1 may be primarily associated with the high-PANscore group, while PANcluster 2 may be mainly associated with the low-PANscore group. In clinical practice, the integration of PANclusters and PANscore not only captures overall features but also facilitates prognostic prediction. Nevertheless, the inherent relationship between the two classification systems warrants further validation in prospective multicenter cohorts, as well as assessment of its robustness across different cancer types and under various treatment contexts, such as immunotherapy and targeted therapy. In summary, the combined application of PANcluster and PANscore provides a novel tool for precise stratification of KIRC; however, its translation into clinical practice requires further support from prospective studies and functional experiments.

In the treatment of KIRC, the expression levels of immune checkpoint molecules significantly influence the efficacy of immunotherapy. Our study found that checkpoint molecules such as CD28, TNFRSF18 (GITR), CTLA4, CD276, and ICOS were upregulated in the high-risk group, which also exhibited higher TIDE scores, immune dysfunction, and an attenuated immune status. These findings suggest that patients in the high-PANscore group may derive greater benefit from immune checkpoint inhibitor therapy. Furthermore, the elevated expression of co-stimulatory molecules including CD28, TNFRSF18, and ICOS in the high-PANscore group implies that the tumor microenvironment in this subgroup may contain abundant infiltrating T cells continuously activated by tumor antigens. However, the concurrent upregulation of inhibitory immune checkpoints such as CTLA4 and CD276 indicates that these activated T cells may subsequently enter an exhausted state, and the immunosuppressive effect is likely mediated predominantly by surface checkpoint molecules, suggesting a relatively single pathway for immune evasion. Research indicates that low CD28 expression can enhance CD8+ILT2+ T cell function, but this effect is inhibited by the HLA-G/ILT2 pathway, rendering HLA-G/ILT2-targeted inhibitors potentially ineffective for KIRC patients with high CD28 expression[49]. Furthermore, GITR agonist antibodies may improve the tumor immune response in KIRC treatment[50]. Additionally, the combination of anti-PD-1 and anti-CTLA4 antibodies is considered in the treatment of metastatic renal cell carcinoma [51]. In KIRC, CD276 shows a stronger correlation with EMT characteristics compared to other checkpoints like PD-L1 and CTLA4, suggesting it may be a key immunotherapy target, especially for KIRC patients unresponsive or resistant to traditional inhibitors[52]. Another study found that CD276 expression is significantly correlated with PD-L1 and associated with a poorer prognosis, further supporting CD276 as a potential immunotherapy target in KIRC. Overall, these results highlight the complex roles of immune checkpoint molecules in KIRC immunotherapy and underscore the importance of personalized

medicine. Despite the high-PANscore group exhibiting a significantly enhanced baseline immunosuppressive microenvironment and a worse natural prognosis, this subgroup may still harbor sufficient $CD8^+$ T cell infiltration reserves, accompanied by marked upregulation of multiple targetable immune checkpoint molecules and low levels of T cell exclusion. This suggests that the immunosuppressive pattern in this group is predominantly characterized by T cell functional exhaustion rather than a lack of T cell infiltration. Based on the above analysis, we propose a precise immunotherapeutic stratification strategy. Patients in the high-PANscore group present with an impaired immune status, corresponding to an immune "desert" or "exhausted" microenvironment. These patients may be resistant to immune checkpoint inhibitor (ICI) monotherapy, such as anti-PD-1/PD-L1 agents, and thus a combination strategy is recommended: first, employ PANoptosis pathway inhibitors (e.g., RIPK1 inhibitors, caspase inhibitors) or immune agonists to remodel the microenvironment, followed by combination with ICI therapy. Under ICI intervention, the exhausted $CD8^+$ T cells within the tumor microenvironment are expected to be effectively reactivated and their cytotoxic function restored, potentially conferring more significant clinical survival benefits compared to the low-risk population. In contrast, the PANcluster 2/low-PANscore group retains functional immune infiltration and normal expression of immune checkpoints, representing an immune "hot" microenvironment, and may benefit from ICI therapy or combined chemotherapy. Of course, the conclusions of this study are still based on bioinformatics analyses and retrospective validation using public datasets; the predictive value of our findings requires further verification and consolidation through prospective cohorts, larger independent samples, and in vitro/in vivo experiments.

To further elucidate the immunological characteristics of PANoptosis-related genes in KIRC, we performed a pan-cancer analysis. This study revealed a broad negative correlation between PANscore and immune cell infiltration across 32 cancer types, indicating that the inhibitory effect of PANoptosis on the tumor immune microenvironment is conserved across cancers. We evaluated immune cell infiltration in 32 cancer types using seven different algorithms. The analysis revealed that PANscore was significantly negatively correlated with $CD8^+$ T cells, $CD4^+$ T cells, γδ T cells, Tregs, Tfh cells, B cells, NK cells, macrophages, M1 macrophages, monocytes, neutrophils, and dendritic cells, whereas it was significantly positively correlated with M0 and M2 macrophages, suggesting that PANoptosis substantially influences the tumor immune microenvironment across a wide range of cancers. Different deconvolution algorithms are based on distinct principles (support vector regression, linear least squares, constrained quadratic programming, marker gene enrichment, etc.) as well as different reference gene sets or cell type definitions. A single algorithm is prone to limitations imposed by its prior assumptions, which may lead to underestimation or overestimation of certain immune subsets. To overcome systematic biases inherent in individual tools, we adopted a "multi-tool consensus" strategy: multiple mainstream algorithms were run in parallel, and then the average or the first principal component of the estimates from each algorithm was used as the immune infiltration signature for subsequent analyses. This approach has been widely adopted in immuno-oncology studies and effectively enhances the robustness and biological reliability of infiltration estimates. The results revealed a significant negative correlation between the high-PANscore group and the majority of immune cell types, suggesting that PANoptosis may regulate the immune system in KIRC, and that a high PANscore may indicate an immune evasion state, thereby increasing resistance to immunotherapy. The above immune-related trends were most pronounced in the KIRC training cohort, while their extent in other cancer types may be modulated by tissue-specific oncogenic drivers and local stromal components, indicating potential inter-cancer heterogeneity in the interaction between PANoptosis and the tumor microenvironment. Given that currently there is no uniformly processed pan-cancer immunotherapy transcriptomic dataset that matches the specific PANscore formula used in this study, we have not performed explicit stratification by immunotherapy response. However, based on the immune features observed in the KIRC cohort, we conceptually discuss how this immunologically dysfunctional phenotype may theoretically predict poor responses to immune checkpoint inhibitors, thereby providing a framework for future validation across various cancer types.To evaluate the prognostic accuracy of PANoptosis-related genes in KIRC, this study compared three traditional machine learning algorithms—LASSO regression, random forest, and SVM-RFE—with CNN. The results demonstrated that CNN achieved an AUC of 0.96 on the test set, significantly outperforming LASSO (AUC = 0.630), random forest (AUC = 0.587), and SVM-RFE (AUC = 0.601). This advantage stems from CNN's deep learning capability, which enables automatic extraction of complex data features and learning of hierarchical structures, effectively capturing non-linear relationships and high-order interactions among genes.

The application of CNN to genomic data requires careful consideration. Genomic data are inherently one-dimensional vectors; however, genes are involved in complex co-expression networks and pathway regulatory relationships, and their expression patterns are not mutually independent. To fully leverage CNN's local receptive fields and parameter-sharing mechanisms, we performed an outer product operation between the expression profiles of the 7 core genes and the infiltration abundances of 10 immune cell types for each sample, constructing a 19×10 two-dimensional feature matrix to characterize the weighted activity of genes under specific immune contexts. This heatmap input was generated by sample-wise independent computation, without any cross-sample normalization, scaling, or feature selection, and without borrowing any inter-sample or cohort-wide statistics throughout the entire process. Heatmaps for the test set and training set were constructed independently using the exact same procedure, fundamentally eliminating the risk of data leakage.

The model was built using the Keras Sequential API, with an input layer of size $(19, 10, 1)$. The convolutional layer was configured with 16 filters of 3×3 kernels (stride 1, same padding, ReLU activation). After flattening, a fully connected layer with 16 neurons (ReLU activation, dropout rate 0.3) was added, followed by an output layer with 1 neuron (sigmoid activation) to output the five-year mortality probability. The data were split into training and internal validation sets at an 8:2 ratio. Hyperparameters were optimized via random search (search space including number and size of convolutional filters, number of neurons in the fully connected layer, learning rate, dropout rate, and batch size), with the optimal combination determined by maximizing the AUC on the validation set. Within the training set, 10-fold cross-validation was implemented, and multiple regularization strategies were applied (dropout rate = 0.3, L2 regularization $\lambda = 0.001$, early stopping monitoring validation loss with a patience of 15 epochs) to

ensure that the model captured genuine prognostic patterns rather than noise in the training data.

CNN integrates two orthogonal data modalities—gene expression and immune infiltration—into a structured spatial matrix, enabling detection of local correlated expression patterns and immune infiltration features that are difficult to identify using traditional linear or tree-based models. All 7 core genes were stringently screened by univariate Cox regression and LASSO regression, demonstrating strong relevance to programmed cell death and robust prognostic predictive performance, with inherently high signal strength. The fact that traditional models performed modestly while CNN excelled precisely reflects its efficient utilization of combined gene-immune information. In this study, the algorithm comparison has an inherent methodological limitation. Traditional machine learning models (LASSO, RF, and SVM-RFE) were trained on gene expression data alone, whereas the CNN model was constructed on a composite matrix combining gene expression and immune infiltration abundance. Thus, the input feature spaces differed between the two approaches, making the comparison not strictly equivalent. The apparently superior performance of CNN may therefore be partly attributable to its access to multimodal features rather than to its network architecture per se. Future studies using identical input features and larger independent cohorts are needed to determine whether CNN truly offers architectural advantages.

Nevertheless, we fully recognize that the current independent validation set has a limited sample size, and the robustness of the high AUC still requires confirmation in larger cohorts. To this end, we plan to prospectively expand the multi-center independent cohort (target $n \geq 200$) and evaluate the predictive stability of the model at different follow-up time points through nested cross-validation combined with time-dependent ROC analysis. Furthermore, we will assess the consistency of prognostic discrimination in subgroup analyses stratified by different TNM stages, pathological grades, and immunotherapy response statuses. In addition, we will validate model performance across different sequencing platforms (RNA-seq and microarray) as well as in cross-population cohorts of diverse ethnic origins, to systematically confirm its cross-platform robustness and generalizability, and comprehensively evaluate its clinical applicability.

Compared with alternative deep learning architectures, fully connected networks (FCNs) treat each gene–immune cell pair as an independent feature, potentially missing local correlations; Transformer-based models, although powerful, require larger sample sizes for effective training. Given the current sample size constraints, CNN represents a practical solution that balances feature extraction efficacy and computational feasibility. In the future, with larger cohorts, Transformer-based architectures and explainable artificial intelligence approaches should be further explored to gain deeper insights into the key gene–immune interaction patterns underlying CNN decisions and to enhance the biological interpretability of the model.

To evaluate the prognostic accuracy of PANoptosis-related genes in KIRC, three machine learning algorithms and CNN were employed. The results showed that CNN surpassed LASSO, RF, and SVM+RFE in terms of accuracy. This advantage may be attributed to CNN's deep learning capability, which enables automatic extraction of complex features from gene expression data and learning of hierarchical data structures, effectively capturing intricate gene interactions and biological patterns. Furthermore, CNN's proficiency in processing image data offers a potential advantage when analyzing the grid-like structure of gene microarray data.

The major findings of this study provide a basis for several highly translational research directions in future precision therapy for KIRC. First, the identification of two distinct PANoptosis patterns, particularly the immunotherapy-sensitive PANcluster 2, lays the foundation for developing novel molecular classification systems. We propose conducting prospective clinical trials to validate the utility of this classification in guiding immunotherapy selection. Second, the prognostic predictive capability of the PANscore risk scoring system positions it as a promising novel biomarker for patient stratification in clinical trials, and its predictive efficacy warrants evaluation in immunotherapy research. Third, the immune infiltration features revealed by pan-cancer analysis suggest that PANoptosis may influence treatment response by modulating the tumor microenvironment, providing a theoretical basis for developing combination immunotherapy strategies, such as PD-1 inhibitors combined with PANoptosis modulators. Finally, the superior performance of the CNN model supports the integration of deep learning algorithms into future multi-omics prognostic prediction models. We anticipate that the next steps will involve validating these findings in larger prospective cohorts and exploring the molecular mechanisms of PANoptosis through single-cell sequencing and spatial transcriptomics technologies. The ultimate goal is to translate biomarker discovery into clinical application.

Conclusion

In conclusion, we identified two distinct PANoptosis patterns, and in silico analyses suggested that PANcluster 2 may be associated with a potentially more favorable predicted response to immunotherapy; however, this finding is hypothesis-generating and requires experimental and clinical validation. We developed a PANscore based on three key genes—*CASP4*, *E2F1*, and *UNC5B*—that may serve as a potential prognostic biomarker and was associated with predicted immunotherapy response in KIRC in our bioinformatics analyses. However, these findings are based solely on bioinformatics analyses and retrospective data from public databases. Until they are validated by large-scale experimental studies using human clinical specimens, animal models, and prospective cohorts, PANscore should be regarded as a hypothesis-generating tool and a potential prognostic biomarker, rather than a clinically validated biomarker or a mature indicator ready to guide clinical decision-making. Furthermore, to our knowledge, this study is the first to report the immune characteristics of PANoptosis-related mRNA genes in KIRC, conduct pan-cancer analysis, and apply machine learning algorithms and convolutional neural networks to evaluate the predictive accuracy of PANoptosis-related genes for patient outcomes. Our findings suggest that CNN may outperform three machine learning algorithms (LASSO, RF, and SVM+RFE) in terms of accuracy in our dataset; however, larger independent cohort studies are needed to further validate the potential superior performance of the CNN model.

Limitations and Future

Perspectives

This study has several limitations. First, traditional machine learning methods such as LASSO regression, random forest, and SVM-RFE perform well in handling high-dimensional genomic data but may fall short in capturing complex nonlinear relationships and deeper gene–gene interactions. These methods rely on predefined feature selection and model structures, which may not fully reveal the intricate patterns embedded in genomic data. Second, although CNN demonstrates powerful capabilities in processing image and sequence data, its application to genomic data still faces challenges. Genomic data are far more complex than image data, and CNN may require larger datasets and more sophisticated network architectures to adequately learn interactions among genes. Third, this study is based solely on bioinformatics analyses without experimental validation, which limits a deeper understanding of the model's predictive results and confidence in its clinical application. Future research should expand dataset sizes, perform experimental validation, and adopt more advanced methods to address confounding factors and data noise, thereby enhancing model accuracy and reliability.

Specifically, the following limitations are acknowledged: First, this study is retrospective in design, relying solely on transcriptomic data from public databases without incorporating independent prospective cohorts. Heterogeneity exists between TCGA and GEO data in terms of acquisition platforms, batch effects, and clinical handling; although corrections were applied, this may still affect model generalizability. Second, immune cell infiltration abundances were estimated using deconvolution algorithms, which are indirect inferences rather than direct quantification by gold-standard methods such as flow cytometry or immunohistochemistry. Moreover, although the CNN strategy of expanding one-dimensional expression data into a two-dimensional matrix via outer product can capture interaction features, its biological interpretability requires further investigation. Third, traditional machine learning approaches, including LASSO, random forest, and SVM-RFE, depend on predefined feature selection and model architectures, limiting their ability to capture complex non-linear relationships; while CNN can automatically extract high-order features, its application to genomic data remains challenging and requires larger datasets and more complex architectures to fully learn gene-gene interactions. Fourth, although the CNN model exhibited excellent discriminative performance on the independent test set, the validation cohort sample size is limited with insufficient statistical power, and the robustness of the high AUC still requires verification in larger external cohorts. Additionally, the construction of PANscore involved multiple between-group comparisons and model iterations without systematically reporting details of multiple-testing correction, posing a risk of false positives. Finally, the current study lacks in vivo and in vitro functional experiments to validate the causal roles of key PANoptosis genes in KIRC progression, and the potential of the PANscore and CNN model for guiding clinical immunotherapy needs confirmation through prospective clinical trials. Furthermore, direct application of the KIRC-derived model in pan-cancer analyses is subject to cancer-type-specific limitations, and independent large-scale cohort re-training and calibration are required for each cancer type.

Future research will be deepened in the following directions: First, we will expand the independent validation sample size by collecting KIRC patient specimens through multi-center prospective cohorts, using nested cross-validation, and conducting stratified validation across different TNM stages, pathological grades, and immunotherapy response statuses, combined with time-dependent ROC analysis to assess model stability at different follow-up time points, thereby systematically confirming the model's generalizability and clinical applicability. Second, we will integrate single-cell RNA sequencing, spatial transcriptomics, and proteomics technologies to resolve, at single-cell resolution, the cell-type-specific expression of PANoptosis genes and their interaction networks within the tumor microenvironment, and employ explainable artificial intelligence approaches to uncover the key gene–immune interaction patterns underlying CNN decisions. Third, we will combine in vitro and in vivo experimental models to rigorously validate the causal regulatory roles of core PANoptosis genes in KIRC development and progression, and further explore their feasibility as potential therapeutic targets. Fourth, we will conduct prospective clinical studies to evaluate the predictive value of PANscore-based stratification for immune checkpoint inhibitor efficacy and postoperative recurrence risk, advancing the translation of PANoptosis signatures from biomarkers to precision diagnostic and therapeutic strategies.

References

1. SUNG H, FERLAY J, SIEGEL R L, et al. Global Cancer Statistics 2020: GLOBOCAN Estimates of Incidence and Mortality Worldwide for 36 Cancers in 185 Countries [J]. CA Cancer J Clin, 2021, 71(3): 209-49.
2. PONTES O, OLIVEIRA-PINTO S, BALTAZAR F, et al. Renal cell carcinoma therapy: Current and new drug candidates [J]. Drug Discov Today, 2022, 27(1): 304-14.
3. JI Y T, LIU S W, ZHANG Y M, et al. [Comparison of the latest cancer statistics, cancer epidemic trends and determinants between China and the United States] [J]. Zhonghua Zhong Liu Za Zhi, 2024, 46: 1-11.
4. WANG Y Z, HU Y. [Age-period-cohort analysis on kidney cancer mortality trend in China, 1992-2016] [J]. Zhonghua Liu Xing Bing Xue Za Zhi, 2021, 42(3): 508-12.
5. MOCH H, AMIN M B, BERNEY D M, et al. The 2022 World Health Organization Classification of Tumours of the Urinary System and Male Genital Organs-Part A: Renal, Penile, and Testicular Tumours [J]. Eur Urol, 2022, 82(5): 458-68.
6. MOCH H, CUBILLA A L, HUMPHREY P A, et al. The 2016 WHO Classification of Tumours of the Urinary System and Male Genital Organs-Part A: Renal, Penile, and Testicular Tumours [J]. Eur Urol, 2016, 70(1): 93-105.
7. HSIEH J J, PURDUE M P, SIGNORETTI S, et al. Renal cell carcinoma [J]. Nat Rev Dis Primers, 2017, 3: 17009.
8. LI P, WONG Y N, ARMSTRONG K, et al. Survival among patients with advanced renal cell carcinoma in the pretargeted versus targeted therapy eras [J]. Cancer Med, 2016, 5(2): 169-81.

9. LUO D, WANG X, WALKER E, et al. Targeted Chemo-radiotherapy of Prostate Cancer Using Gold Nanoclusters with Protease Activatable Monomethyl Auristatin E [J]. ACS Appl Mater Interfaces, 2022, 14(13): 14916-27.
10. HUANG C P, CHEN J, CHEN C C, et al. ASC-J9(R) increases the bladder cancer chemotherapy efficacy via altering the androgen receptor (AR) and NF-kappaB survival signals [J]. J Exp Clin Cancer Res, 2019, 38(1): 275.
11. SIVA S, KOTHARI G, MUACEVIC A, et al. Radiotherapy for renal cell carcinoma: renaissance of an overlooked approach [J]. Nat Rev Urol, 2017, 14(9): 549-63.
12. DESCHAVANNE P J, FERTIL B. A review of human cell radiosensitivity in vitro [J]. Int J Radiat Oncol Biol Phys, 1996, 34(1): 251-66.
13. ACHARYA N, SINGH K P. Recent advances in the molecular basis of chemotherapy resistance and potential application of epigenetic therapeutics in chemorefractory renal cell carcinoma [J]. WIREs Mech Dis, 2022, 14(6): e1575.
14. HANAHAN D, WEINBERG R A. The hallmarks of cancer [J]. Cell, 2000, 100(1): 57-70.
15. ROYER-POKORA B, BEIER M, BRANDT A, et al. Chemotherapy and terminal skeletal muscle differentiation in WT1-mutant Wilms tumors [J]. Cancer Med, 2018, 7(4): 1359-68.
16. SHUKLA A, NGUYEN T H M, MOKA S B, et al. Chromosome arm aneuploidies shape tumour evolution and drug response [J]. Nat Commun, 2020, 11(1): 449.
17. COURTNEY K D, MA Y, DIAZ DE LEON A, et al. HIF-2 Complex Dissociation, Target Inhibition, and Acquired Resistance with PT2385, a First-in-Class HIF-2 Inhibitor, in Patients with Clear Cell Renal Cell Carcinoma [J]. Clin Cancer Res, 2020, 26(4): 793-803.
18. SENBABAOGLU Y, GEJMAN R S, WINER A G, et al. Tumor immune microenvironment characterization in clear cell renal cell carcinoma identifies prognostic and immunotherapeutically relevant messenger RNA signatures [J]. Genome Biol, 2016, 17(1): 231.
19. CHOUEIRI T K, MOTZER R J. Systemic Therapy for Metastatic Renal-Cell Carcinoma [J]. N Engl J Med, 2017, 376(4): 354-66.
20. MOTZER R J, HUTSON T E, MCCANN L, et al. Overall survival in renal-cell carcinoma with pazopanib versus sunitinib [J]. N Engl J Med, 2014, 370(18): 1769-70.
21. RINI B I, PLIMACK E R, STUS V, et al. Pembrolizumab plus Axitinib versus Sunitinib for Advanced Renal-Cell Carcinoma [J]. N Engl J Med, 2019, 380(12): 1116-27.
22. LAI Y, TANG F, HUANG Y, et al. The tumour microenvironment and metabolism in renal cell carcinoma targeted or immune therapy [J]. J Cell Physiol, 2021, 236(3): 1616-27.
23. RICKETTS C J, DE CUBAS A A, FAN H, et al. The Cancer Genome Atlas Comprehensive Molecular Characterization of Renal Cell Carcinoma [J]. Cell Rep, 2018, 23(12): 3698.
24. [24] BRAUN D A, BAKOUNY Z, HIRSCH L, et al. Beyond conventional immune-checkpoint inhibition - novel immunotherapies for renal cell carcinoma [J]. Nat Rev Clin Oncol, 2021, 18(4): 199-214.
25. DAI S, ZENG H, LIU Z, et al. Intratumoral CXCL13 (+)CD8(+)T cell infiltration determines poor clinical outcomes and immunoevasive contexture in patients with clear cell renal cell carcinoma [J]. J Immunother Cancer, 2021, 9(2).
26. GOLKARAM M, KUO F, GUPTA S, et al. Spatiotemporal evolution of the clear cell renal cell carcinoma microenvironment links intra-tumoral heterogeneity to immune escape [J]. Genome Med, 2022, 14(1): 143.
27. WU X, JIANG D, LIU H, et al. CD8(+) T Cell-Based Molecular Classification With Heterogeneous Immunogenomic Landscapes and Clinical Significance of Clear Cell Renal Cell Carcinoma [J]. Front Immunol, 2021, 12: 745945.
28. MALIREDDI R K S, KESAVARDHANA S, KANNEGANTI T D. ZBP1 and TAK1: Master Regulators of NLRP3 Inflammasome/Pyroptosis, Apoptosis, and Necroptosis (PAN-optosis) [J]. Front Cell Infect Microbiol, 2019, 9: 406.
29. LIU X, MIAO M, SUN J, et al. PANoptosis: a potential new target for programmed cell death in breast cancer treatment and prognosis [J]. Apoptosis, 2024, 29(3-4): 277-88.
30. LEE S, KARKI R, WANG Y, et al. AIM2 forms a complex with pyrin and ZBP1 to drive PANoptosis and host defence [J]. Nature, 2021, 597(7876): 415-9.
31. YI X, LI J, ZHENG X, et al. Construction of PANoptosis signature: Novel target discovery for prostate cancer immunotherapy [J]. Mol Ther Nucleic Acids, 2023, 33: 376-90.
32. ZHANG Z, ZHANG F, PANG P, et al. Identification of PANoptosis-relevant subgroups to evaluate the prognosis and immune landscape of patients with liver hepatocellular carcinoma [J]. Front Cell Dev Biol, 2023, 11: 1210456.
33. PAN H, PAN J, LI P, et al. Characterization of PANoptosis patterns predicts survival and immunotherapy response in gastric cancer [J]. Clin Immunol, 2022, 238: 109019.
34. [LI T, FU J, ZENG Z, et al. TIMER2.0 for analysis of tumor-infiltrating immune cells [J]. Nucleic Acids Res, 2020, 48(W1): W509-W14.

35. RACLE J, DE JONGE K, BAUMGAERTNER P, et al. Simultaneous enumeration of cancer and immune cell types from bulk tumor gene expression data [J]. Elife, 2017, 6.
36. ARAN D, HU Z, BUTTE A J. xCell: digitally portraying the tissue cellular heterogeneity landscape [J]. Genome Biol, 2017, 18(1): 220.
37. NEWMAN A M, LIU C L, GREEN M R, et al. Robust enumeration of cell subsets from tissue expression profiles [J]. Nat Methods, 2015, 12(5): 453-7.
38. FINOTELLO F, MAYER C, PLATTNER C, et al. Molecular and pharmacological modulators of the tumor immune contexture revealed by deconvolution of RNA-seq data [J]. Genome Med, 2019, 11(1): 34.
39. BECHT E, GIRALDO N A, LACROIX L, et al. Estimating the population abundance of tissue-infiltrating immune and stromal cell populations using gene expression [J]. Genome Biol, 2016, 17(1): 218.
40. LIU W, QU C, WANG X. Comprehensive analysis of the role of immune-related PANoptosis lncRNA model in renal clear cell carcinoma based on RNA transcriptome and single-cell sequencing [J]. Oncol Res, 2023, 31(4): 543-67.
41. WANG Y, ZHOU J, ZHANG N, et al. A Novel Defined PANoptosis-Related miRNA Signature for Predicting the Prognosis and Immune Characteristics in Clear Cell Renal Cell Carcinoma: A miRNA Signature for the Prognosis of ccRCC [J]. Int J Mol Sci, 2023, 24(11).
42. LABROUSSE-ARIAS D, MARTINEZ-ALONSO E, CORRAL-ESCARIZ M, et al. VHL promotes immune response against renal cell carcinoma via NF-kappaB-dependent regulation of VCAM-1 [J]. J Cell Biol, 2017, 216(3): 835-47.
43. BRAUN D A, HOU Y, BAKOUNY Z, et al. Interplay of somatic alterations and immune infiltration modulates response to PD-1 blockade in advanced clear cell renal cell carcinoma [J]. Nat Med, 2020, 26(6): 909-18.
44. LIN K, CHEN H, SU C, et al. Long Non-Coding RNA TTN-AS1 Serves as a Competing Endogenous RNA of miR-195 to Facilitate Clear Cell Renal Cell Carcinoma Progression [J]. Cancer Manag Res, 2020, 12: 3091-7.
45. FU L, BAO J, LI J, et al. Crosstalk of necroptosis and pyroptosis defines tumor microenvironment characterization and predicts prognosis in clear cell renal carcinoma [J]. Front Immunol, 2022, 13: 1021935.
46. CHEN R, ZHANG Z, HU B, et al. Identification of the Expression and Clinical Significance of E2F Family in Clear Cell Renal Cell Carcinoma [J]. Int J Gen Med, 2022, 15: 1193-212.
47. ZHAN B, KONG C, GUO K, et al. PKCalpha is involved in the progression of kidney carcinoma through regulating netrin-1/UNC5B signaling pathway [J]. Tumour Biol, 2013, 34(3): 1759-66.
48. PRAJAPATI K, YAN C, YANG Q, et al. The FLRT3-UNC5B checkpoint pathway inhibits T cell-based cancer immunotherapies [J]. Sci Adv, 2024, 10(9): eadj4698.
49. DUMONT C, JACQUIER A, VERINE J, et al. CD8(+) PD-1(-)ILT2(+) T Cells Are an Intratumoral Cytotoxic Population Selectively Inhibited by the Immune-Checkpoint HLA-G [J]. Cancer Immunol Res, 2019, 7(10): 1619-32.
50. MOLLICA V, DI NUNNO V, GATTO L, et al. Novel Therapeutic Approaches and Targets Currently Under Evaluation for Renal Cell Carcinoma: Waiting for the Revolution [J]. Clin Drug Investig, 2019, 39(6): 503-19.
51. PADERI A, GIORGIONE R, GIOMMONI E, et al. Association between Immune Related Adverse Events and Outcome in Patients with Metastatic Renal Cell Carcinoma Treated with Immune Checkpoint Inhibitors [J]. Cancers (Basel), 2021, 13(4).
52. LIANG J, LIU Z, ZOU Z, et al. The Correlation Between the Immune and Epithelial-Mesenchymal Transition Signatures Suggests Potential Therapeutic Targets and Prognosis Prediction Approaches in Kidney Cancer [J]. Sci Rep, 2018, 8(1): 6570.

DECLARATIONS

Ethics approval and consent to participate

Not applicable.

Clinical trial number

Not applicable.

Consent to Participate declaration

Not applicable

Consent for publication

All authors agree to publication.

Date availability statement

The detailed description of data availability can be found at the following links: TCGA-KIRC cohort (https://portal.gdc.cancer.gov/projects/TCGA-KIRC), GSE29609 (https://www.ncbi.nlm.nih.gov/geo/query/acc.cgi).

Competing interests

No, We declare that the authors have no competing interests, or other interests that might be perceived to influence the results and/or discussion reported in this paper.

Author Contribution declaration

Lixiong Zeng and Houyu Gan conceived and supervised the entire project. Qiuli Chen and Delin Liu wrote the code and drafted the manuscript. Qian Guo and Fanyan Ou processed the data and analyzed the results. Jie Yang and Kanglai Wei improved the algorithms and reviewed the manuscript. All authors discussed, revised, and proofread the manuscript. The

authors wish to acknowledge that Lixiong Zeng, Houyu Gan, Qiuli Chen contributed equally to this work and are considered co-first authors. Fanyan Ou, Jie Yang and Kanglai Wei are co-corresponding authors.

Funding Declaration

This work was supported by Guangxi Medical University Youth Science Project (No.GXMUYSFB2026057).

Acknowledgements

The authors acknowledge the technical support provided by the Guangxi Key Laboratory of Intelligent Precision Medicine and Guangxi Anrenxin Biotechnology Co., Ltd.